

Study on a vibratory tri-axis MEMS gyroscope with single drive and multiple axes angular rate sense

Zhang Tingkai · Xing Chaoyang ·
Zhang Ling · Wang Wei

Received: 9 August 2014 / Accepted: 26 August 2014 / Published online: 11 September 2014
© Springer-Verlag Berlin Heidelberg 2014

Abstract In this paper a vibratory tri-axis gyroscope with single drive and three axes angular rate sense is presented. Firstly the structural design is proposed. And based on the modal analysis of this structure the operating principle of gyroscope is explained. Secondly the detail design of this gyroscope is presented. Based on simulation, the performance of the gyroscope is evaluated, the character of structural coupling among the drive and sense modes is studied. Thirdly the SOI fabrication process for this gyroscope is described. Fourthly the circuitry design including AGC and PLL is discussed, and the signal process is described in detail. Finally the implementation of this gyroscope is presented. Experiment results show the performance of the gyroscope. The scale factors are -0.0078 V/°/s, -0.0043 V/°/s and -0.0049 V/°/s along X-, Y- and Z-axis respectively. And experiment results also indicate the character of structural coupling among the drive and sense modes similar with the results of simulation.

1 Introduction

Tri-axis MEMS gyroscope, with high integration and multiple function sensing three axes angular rate simultaneously, attracts a lot of attention nowadays. Besides, tri-axis MEMS gyroscope also has advantages such as low cost and tiny size, so it can be applied widely in industries, including gaming, image stabilization, body-motion dynamics, dead reckoning for location-based services and electronic stability

control. Unfortunately the development of tri-axis MEMS is relatively slower than that of single axis MEMS gyroscope because of the difficulty in fabrication and complexity in design.

Several types of tri-axis gyroscope have been presented so far. For instance, Chou and Chang (1997) and Chou et al. (1999) reported a hemispherical shell gyroscope that can sense three axes angular rate simultaneously. But this type of gyroscope need complicate 3-D manufacturing process and is not compatible to the popular MEMS process nowadays. Okada et al. (2003) proposed a cuboid-shaped gyroscope with high sensitivity and low cross-talk sensitivity. But this gyroscope need be manufactured by complicated process and it is difficult to decrease its cost. In Ref. John and Vinay (2006), reported a tri-axis micro-gyroscope with only a single proof mass as the detection element. However, the coupling effects will be considerable and need to be effectively reduced at first. There are also tri-axis micro-gyroscope based on other concept, such as the case reported in Ref. (Dao et al. 2007; Zhu et al. 2006), where the author proposed a gyroscope with non-vibrating structure. But this gyroscope is also not suitable to be fabricated by a relative simple process. Johari et al. (2008) reported a single-disk tri-axis gyroscope. The disk-shaped gyroscope works normally in conditions of high-order mode and limited vibrating amplitude, so it will be complex to design the processing circuits. Tsai and Sue (2008a, b, 2010) and Tsai et al. (2009) proposed a tri-axis gyroscope based on distributed translational proof mass. This gyroscope is suitable to be manufactured by conventional SOI fabrication process, and is improved in drive efficacy.

Though there are a few reported tri-axis gyroscopes, the key issues are not studied sufficiently, Such as the structural

Z. Tingkai (✉) · X. Chaoyang · Z. Ling · W. Wei
Beijing Institute of Aerospace Control Instrument,
100094 Beijing, China
e-mail: billmetre@aliyun.com

coupling among the drive and sense modes. In our previous work, the design of a tri-axis gyroscope with single drive and multiple angular rate sense is proposed (Zhang and Wang 2012). In this paper, the implement of this gyroscope is presented in detail. The performance is evaluated by experiments, the character of structural coupling among drive and sense modes is study by both simulation and experiment.

2 Operating principle

Figure 1 shows the design of the triple-axis MEMS gyroscope and Fig. 2 shows the mode shape of drive mode and sense modes of three perpendicular axes of this structure. In this structure there are four proof masses designed for sensing the rotation along X-axis and Y-axis in-plane.

Fig. 1 Design of the tri-axis gyroscope

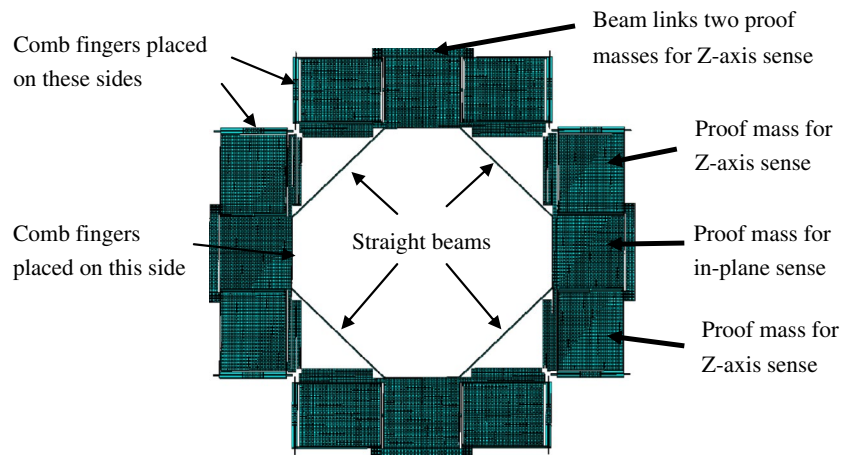
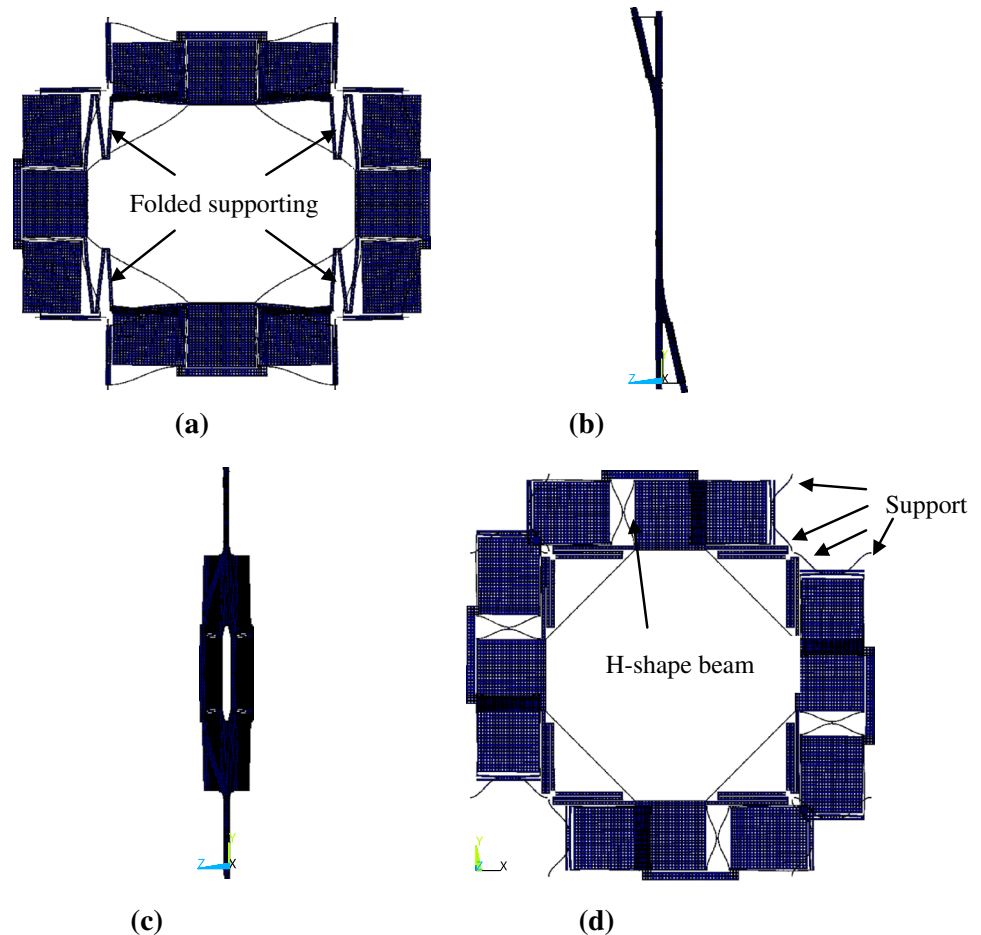


Fig. 2 The drive and sense mode shapes of the structure. **a** Drive mode. **b** X-axis sense mode. **c** Y-axis sense mode. **d** Z-axis sense mode



The four proof masses are linked together by four straight beams, and are supported by four folded beams. There are also eight proof masses designed for sensing rotation along Z-axis. The eight proof masses are linked to the four proof masses for in-plane sense through eight H-shape beams, and are supported by straight beams. Of the eight proof masses for Z-axis sense the two proof masses linked to the same proof mass for in-plane sense are linked together.

There are comb capacitors placed inside the structure parallel to four sides of the four proof masses for in-plane sense. When applied altering voltage with frequency same as that of its drive mode, the structure is driven vibrating at its natural frequency. The two proof masses placed along the same axis (X- or Y-axis) are vibrating inward or outward simultaneously. And when this two proof masses moving inward, the other two proof masses moving outward. The eight proof masses for z-axis sense are

driven vibrating among the other four proof masses by the H-shape beams.

The vibrating driven by Coriolis force when gyroscope rotates along three axes is measured by the change of capacitors. There are plane capacitors formed by the proof masses and metal layers on substrate to measure rotation along X- or Y-axis in-plane. And there are capacitors designed on the eight proof masses to measure rotation along Z-axis.

3 Structure design and simulation

The structure is designed with dimensions about 5 mm × 5 mm in area. And the drive mode and three sense modes' frequencies are matched to about 8,820 Hz. The area of the four masses for in-plane sense is about 1 mm × 1 mm, and that of the other eight masses is about 0.67 mm × 0.8 mm.

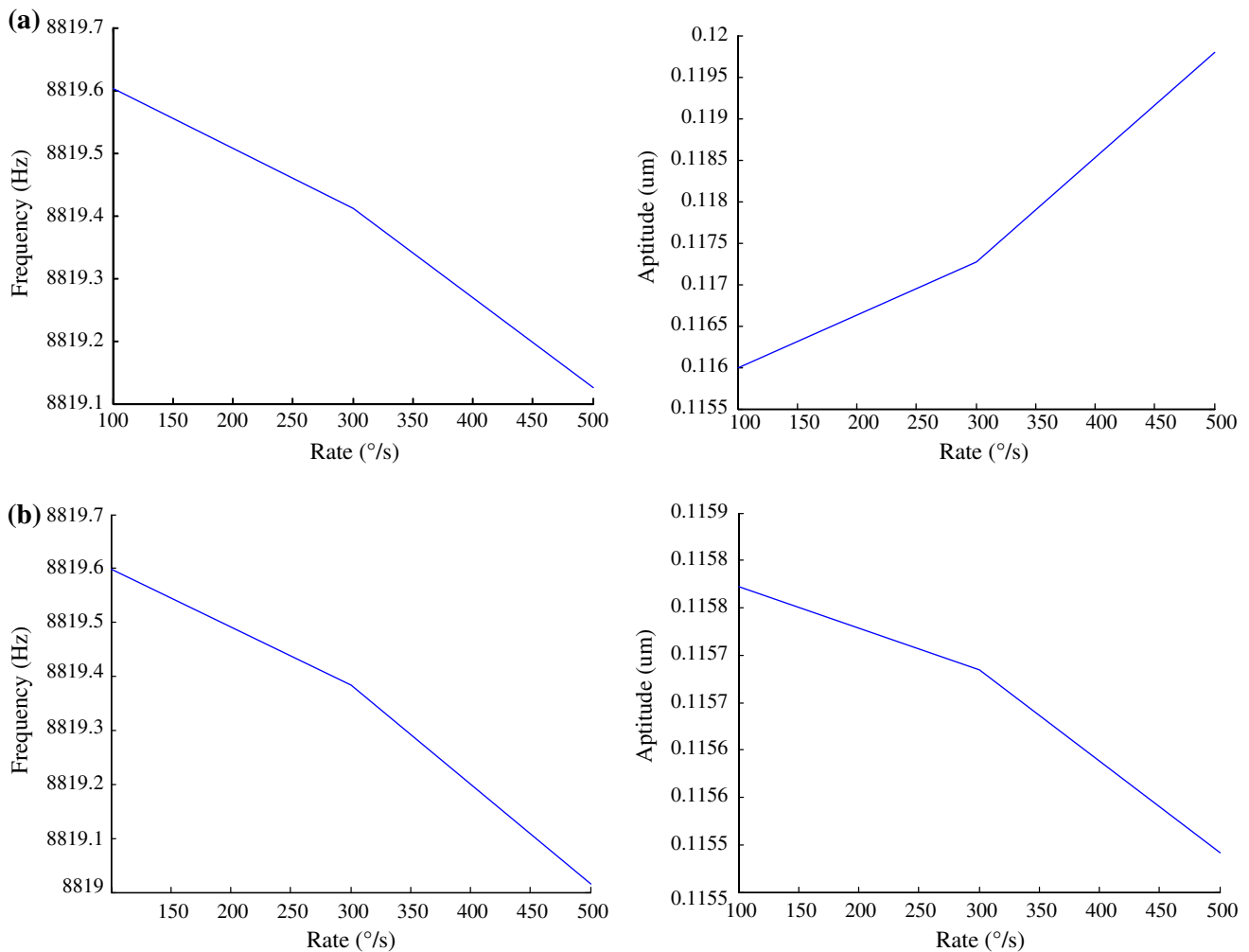


Fig. 3 Effect of structure rotating along single axis on the work frequency and aptitude (where only the cases when gyroscope rotates forward are shown, the case of rotating reverse will be the same). **a** Curve of work frequency and aptitude when structure rotating along

X-axis (the case along Y-axis will be the same for the structure is symmetric). **b** Curve of work frequency and aptitude when structure rotating along Z-axis

The structure is made in silicon, and is bonded with substrate of glass. The thickness of the structure is designed to 56 μm , and the clearance between silicon and substrate is designed to 4 μm . There are electrode pads designed around the structure on bonded surface of glass as the ports to link to circuitry system.

As elastic structure, when rotating the natural frequencies of both drive mode and sense modes of gyroscope will be affected by spinning soft and coriolis effect. The work frequency of the gyroscope so will shift when working at its natural frequency. And so the output of gyroscope will be affected consequently.

The shift of natural frequency and the consistent aptitude of the drive mode under the same drive level are shown in Fig. 3. From Fig. 3, the drive frequency of drive mode decreases and the aptitude increase when rotating along single axis in-plane. And both the frequency and the aptitude decrease when rotating along Z-axis.

When rotating along two axes simultaneously, the change of drive frequency and aptitude of gyroscope are shown in Fig. 4. As are seen, the drive frequency decreases when rotating along every two axes. And the change of aptitude combines the changes along both axes respectively.

The changes of the sense capacitors, as the output of gyroscope, are calculated according to the relative displacement of the structure driven by coriolis force when the gyroscope rotates. Figure 5 shows the curves of output and scale factor of the gyroscope along three axes. The output along certain axis is calculated under condition that gyroscope rotating along one certain perpendicular axis at a series of rotation rate. The changes of scale factors of three axes are also calculated. As shown in Fig. 5 the scale factors of three axes all decrease when gyroscope rotating along another perpendicular axis. And the greater the gyroscope rotates along one certain axis, the smaller the scale factor of another perpendicular axis.

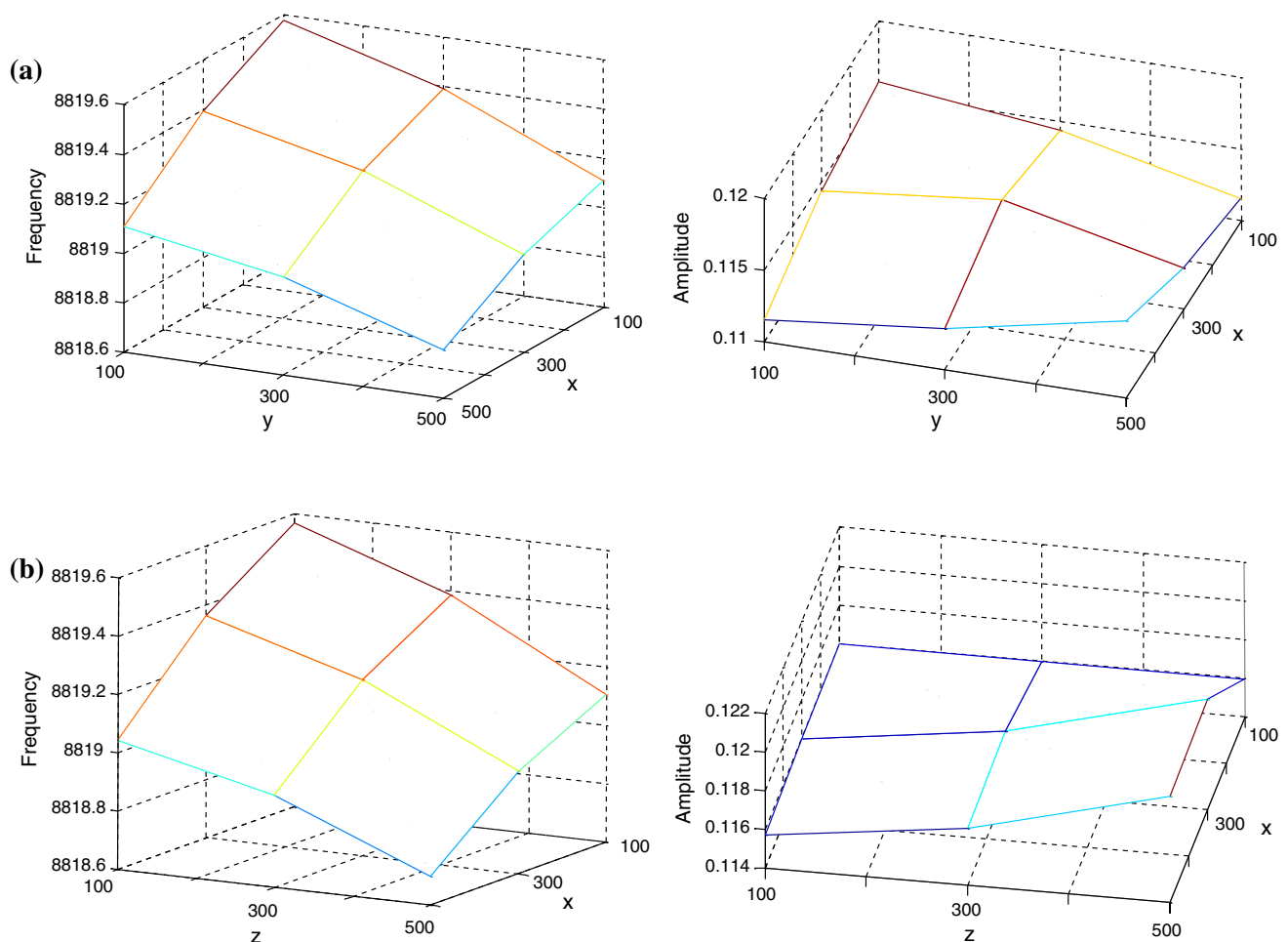


Fig. 4 Effect of structure rotating along two axes simultaneously on the work frequency and aptitude (where only the cases when gyroscope rotates forward are shown, the case of rotating backward will be the same). **a** Plot of work frequency and aptitude when structure

rotating along both X-axis and Y-axis. **b** Plot of work frequency and aptitude when structure rotating along both Z-axis and X-axis (the case along both Z- and Y-axes will be the same for the structure is symmetric)

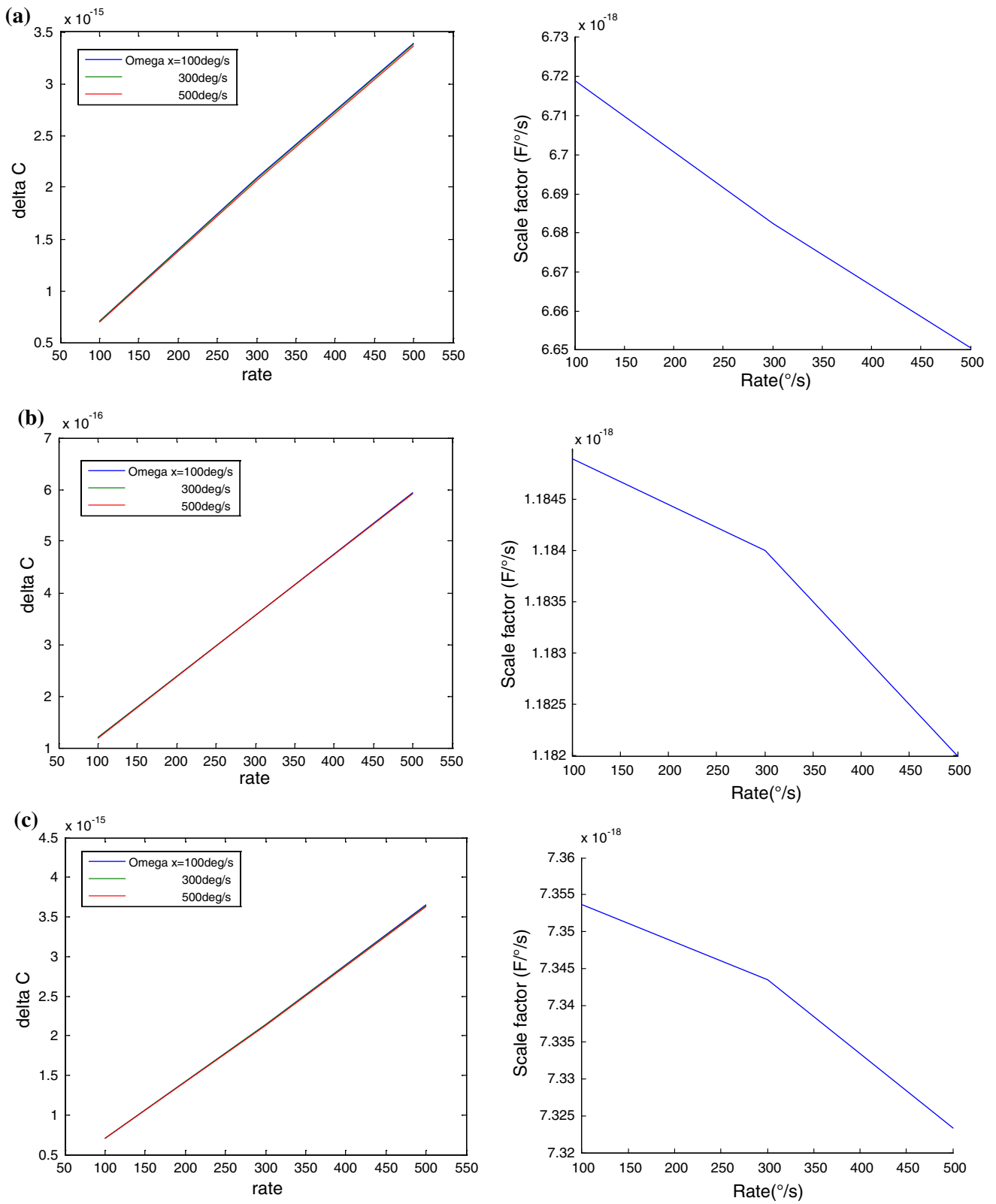


Fig. 5 Curves of capacitor change and scale factor (where only the scale factors when gyroscope rotates forward among other axis are shown, the case of rotating backward will be the same). **a** Effect of

X-axis rotation on output of Y-axis. **b** Effect of X-axis rotation on output of Z-axis. **c** Effect of Z-axis rotation on output of X-axis

Fig. 6 MEMS fabrication process of structure

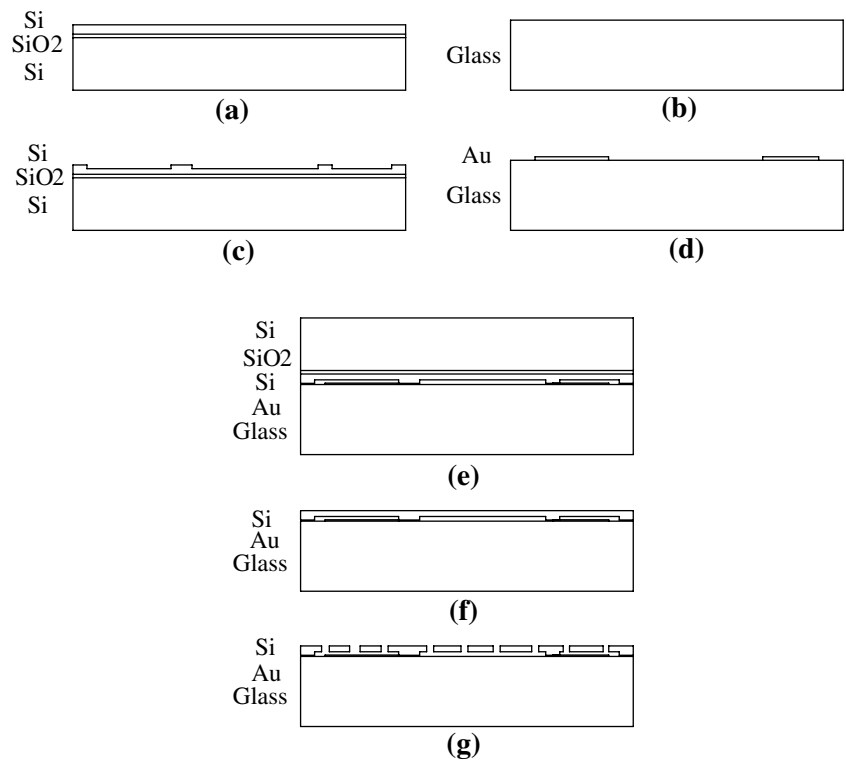
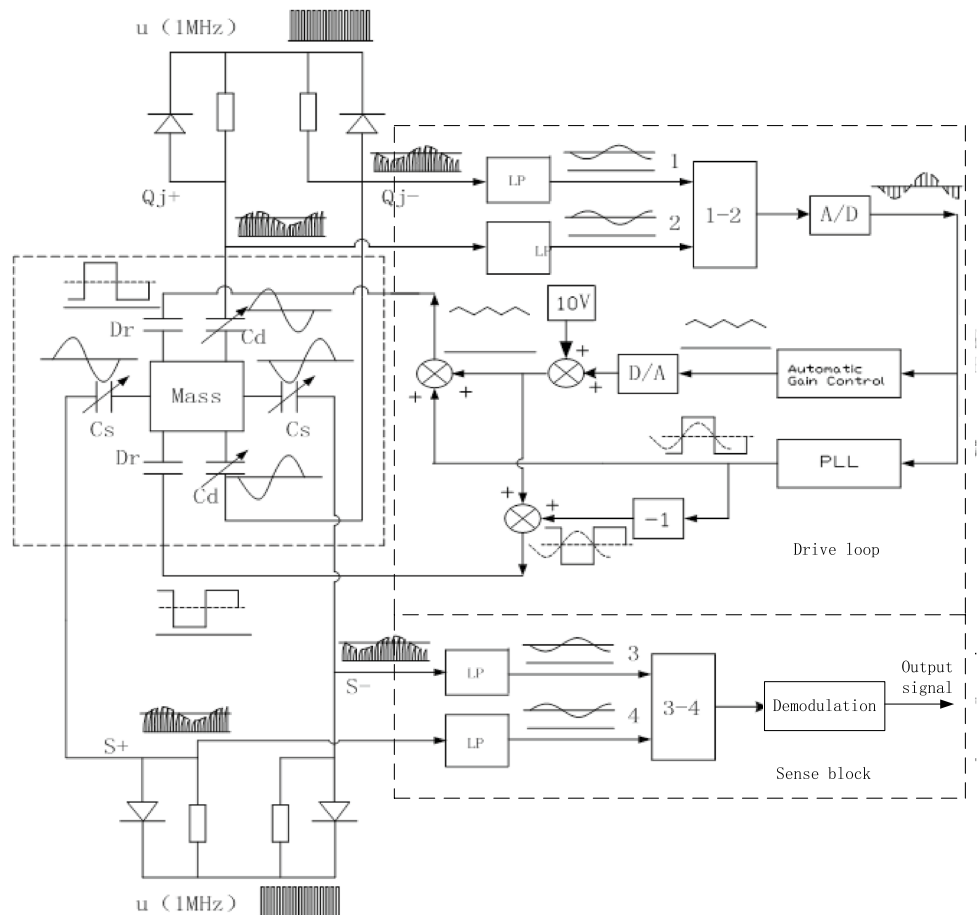


Fig. 7 The schematic block diagram of circuitry system (for simplification only one sense block shown for other two are as the same)



4 Fabrication process

The structure is fabricated by a MEMS fabrication process described in Fig. 6. The SOI wafer with a structure layer of 60 μm thickness is used to fabricate gyroscope's structure, and the glass wafer is used as the substrate to support the gyroscope's structure. In this fabrication process, firstly, the SOI wafer is etched on its structure layer forming bonding area, and the glass is deposited metal layer and then the metal layer is etched to form electrodes and pads, as shown in Fig. 6a–d. Then the SOI wafer and glass are bonded together by anodic bonding, as shown in Fig. 6e. After the bonding process the substrate of the SOI is etched thoroughly in KOH, and the SiO_2 layer is removed by HF, as shown in Fig. 6f. Finally the silicon layer is etched by ICP to release the gyroscope's structure, as shown in Fig. 6g.

5 Circuitry design

Figure 7 shows the schematic block diagram of the gyroscope's circuitry system. In this system an AGC (Automatic Gain Control) and a PLL (Phase Lock Loop) are used to keep the gyroscope vibrate at its natural frequency and constant amplitude. As shown in Fig. 7, the movable electrodes for drive-mode of the gyroscope are electrically linked to C/V module. When vibrating the movement of the electrodes of gyroscope modulate the amplitude of high

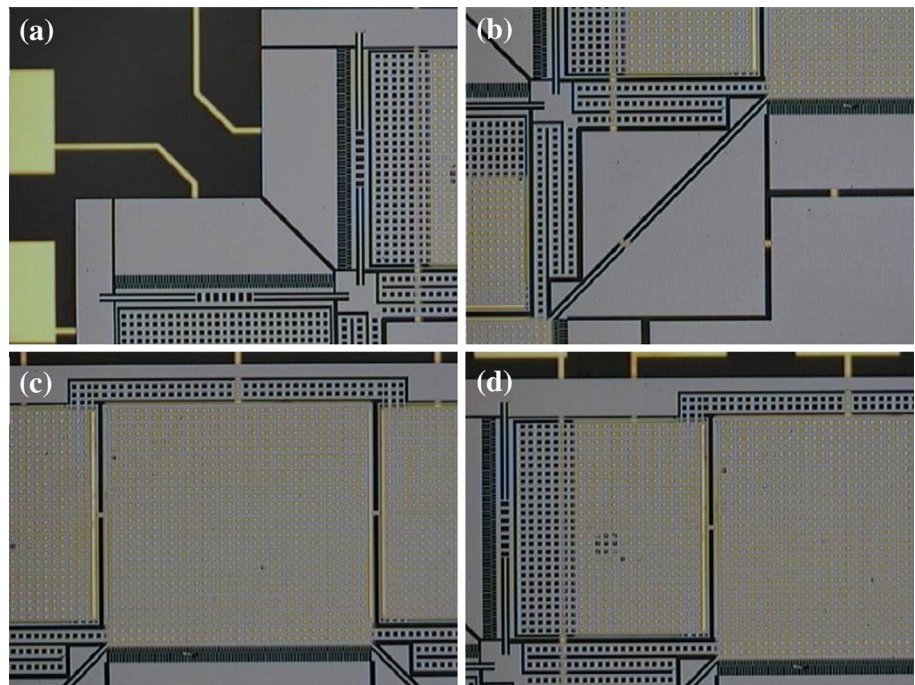
frequency signal at the frequency of gyroscope's vibration. The modulated high frequency signal was filtered by low-pass filter. After a differential module the amplitude of measurement signal is doubled. The measurement signal is then used to control the amplitude and the frequency of the gyroscope's vibration through AGC and PLL respectively. AGC adjusts the high DC voltage through an adjustment signal calculated according to the difference between the amplitude of the measurement signal and a predetermined DC voltage. PLL tunes the frequency of the drive signal until the output signal 90° after the drive signal in phase. The drive signal and its coherent signal with 180° phase transfer are combined with the adjusted high DC voltage. And the combination signals drive the gyroscope to work normally.

Similarly with drive movement, the change of the sense capacitors are measured by C/V module. After being filtered by low pass and differential module the measurement signal is demodulated by the drive signal. The demodulated signal is then filtered by low pass and amplified as the final output signal of the gyroscope.

6 Implementation and experimental results

Figure 8 shows the pictures of the structure of the gyroscope. This structure is packaged into ceramics package and then is integrated into PCB. Agilent 35670 is used here to measure the frequency response of the structure. And

Fig. 8 Pictures of the structure



X5

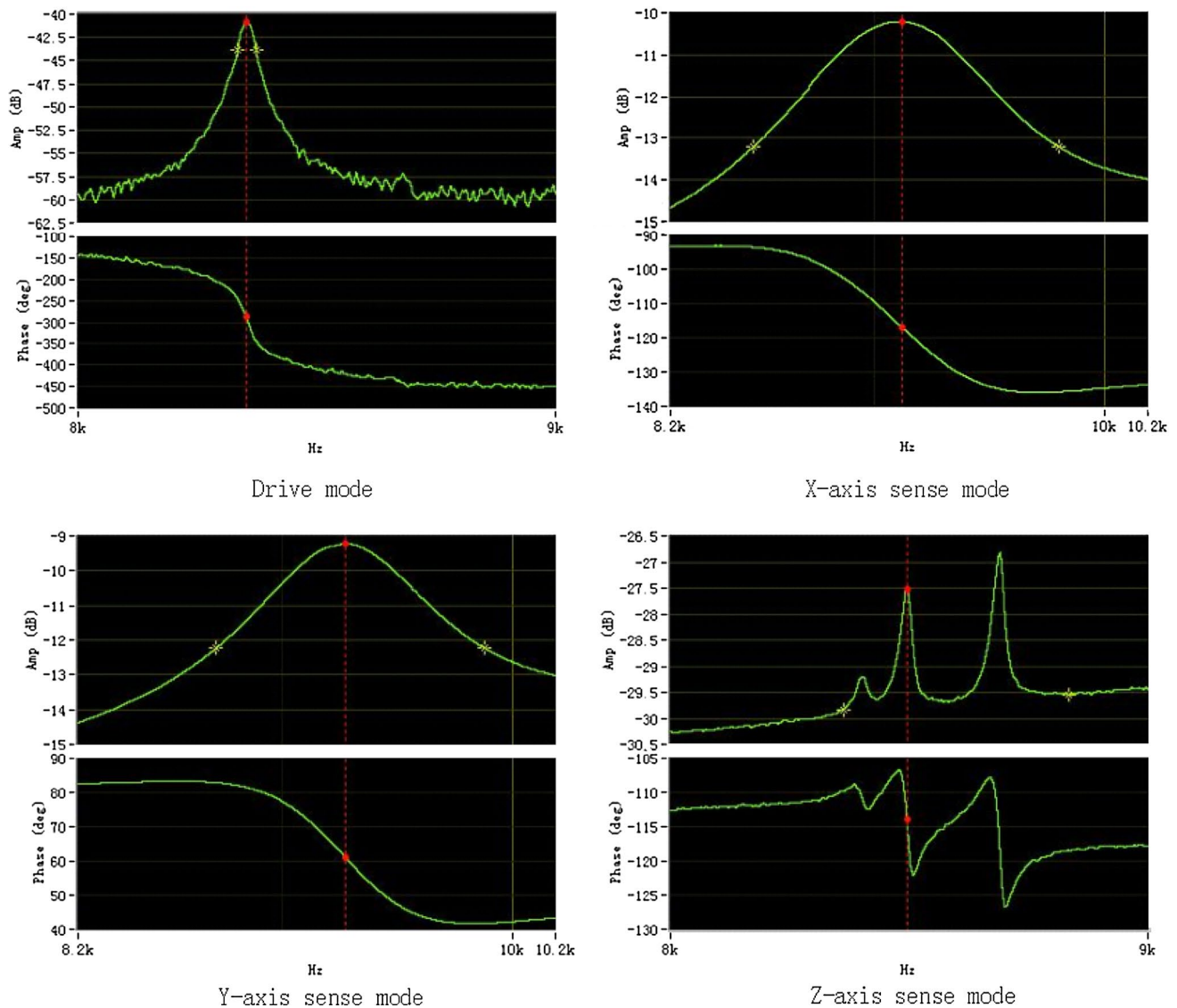


Fig. 9 Frequency response of the structure

the frequency response of the structure is shown in Fig. 9. In Fig. 9, (a) shows the frequency response of the drive mode, (b) and (c) show the frequency responses of the sense modes to sense rotation in-plane, and (d) shows the frequency response of sense mode to sense rotation along Z-axis.

The gyroscope is examined and evaluated by experiments. The prototype of gyroscope is made up by integrating the sense structure with PCB. The output scale factor and nonlinearity is measured by a two-axis rate table, as shown in Fig. 10. The two-axis rate table is made up by two single axis spinners. The top spinner is fixed on the plane of another spinner (named bottom spinner). The two spinners can work independent on each others. The gyroscope is installed on the plane of the rate table, as shown in Fig. 10, when the top spinner rotates only, the output of

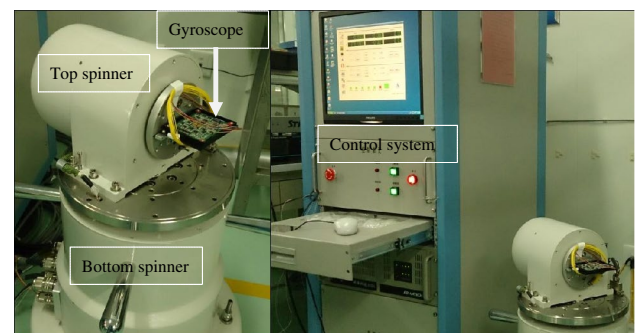


Fig. 10 Rate table equipment used to test gyroscope

the gyroscope when rotating along certain single axis can be measured. Figure 11 shows the results of the gyroscope only along X-, Y- and Z-axis respectively. The scale factors

of the gyroscope along three axes are about $-0.0078 \text{ V}/^\circ/\text{s}$, $-0.0043 \text{ V}/^\circ/\text{s}$ and $-0.0049 \text{ V}/^\circ/\text{s}$, and the nonlinearities are 5.37, 4.91 and 8.66 ‰ along X-, Y- and Z-axis respectively.

When two spinners work rotating simultaneously, the coupling character between any two axes of gyroscope can be measured. When the top spinner rotates at certain rate, and the bottom spinner rotates at series of speeds at the range of gyroscope, the scale factors of two axes perpendicular with the axis parallel to the rotating axis of the top spinner of gyroscope are measured. For instance the gyroscope is fixed on the top spinner and its X-sense axis is parallel to the rotating axis of top spinner, when two spinner rotate simultaneously, the output along Y- and Z-axis of gyroscope alter periodically. And when X–Y plane of gyroscope parallel to the plane of the bottom spinner, the Z-axis output of gyroscope become its maximum and the Y-axis output is at its zero rate output. When X–Y plane of gyroscope perpendicular to the plane of the bottom spinner, the Y-axis output of gyroscope become its maximum and the

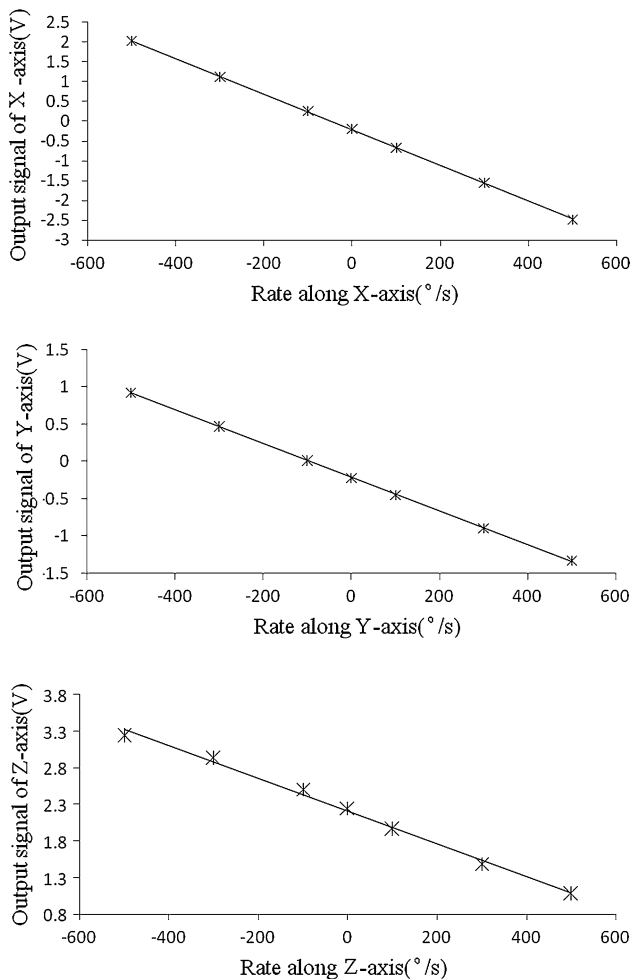


Fig. 11 The output curves along three axes of gyroscope

Z-axis output is at its zero rate output. The amplitude of the output then is calculated as the output of gyroscope along Y- and Z-axes. By this way the output of Y- and Z-axes

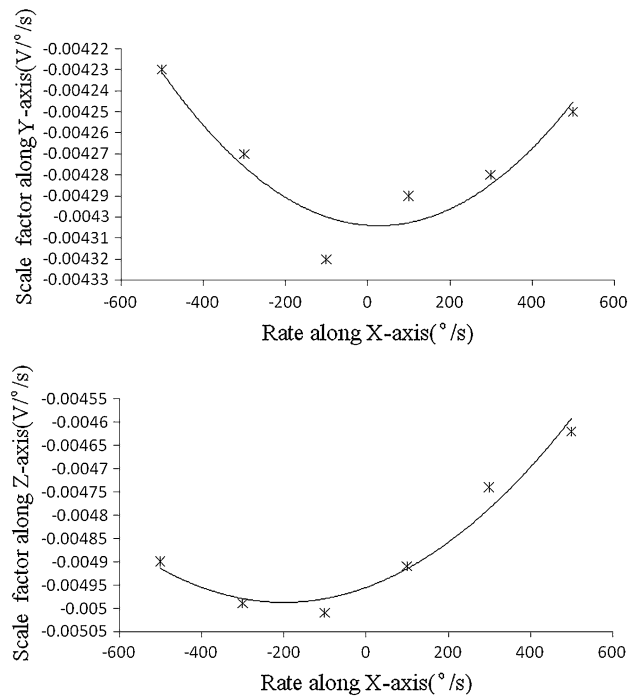


Fig. 12 Effect by rotating along X-axis on scale factor of Y- and Z-axes

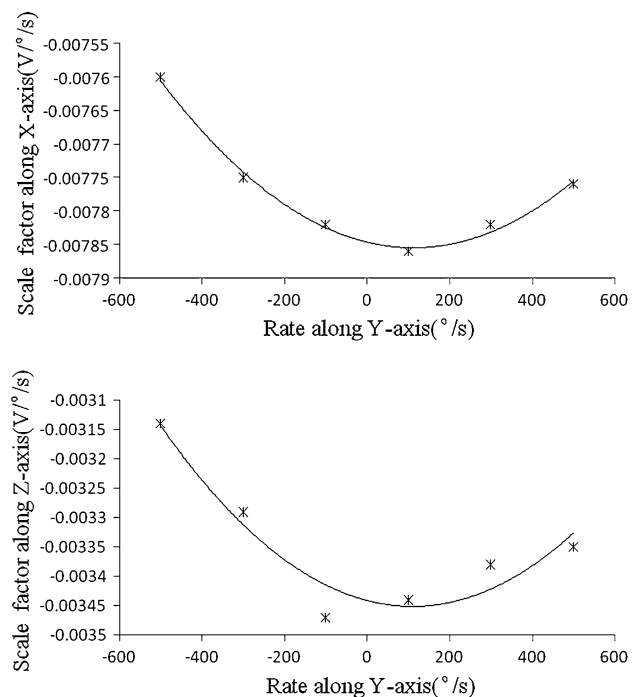


Fig. 13 Effect by rotating along Y-axis on scale factor of X- and Z-axes

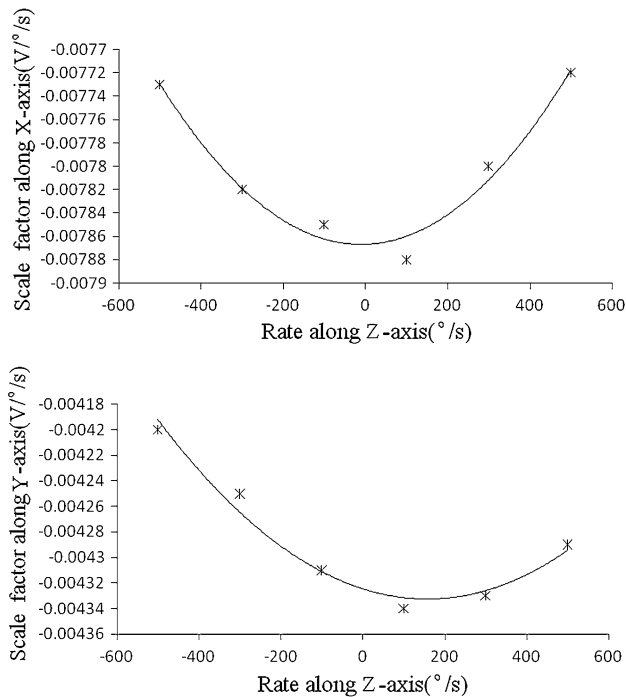


Fig. 14 Effect by rotating along Z-axis on scale factor of X- and Y-axes

when gyroscope rotates at different rate along X-axis are measured. Figures 12, 13, and 14 show the curves of scale factors of every axis of gyroscope that affected by rotation along other perpendicular axis. From those curves, the absolute value of scale factor along certain axis is decrease when gyroscope rotates along any other perpendicular axis. And the scale factor will be its maximum when rotates along single axis. Theoretically, the scale factor will be the same when gyroscope rotates forward and backward at the same rate. But in our experiment, it is not the case as shown in Figs. 12, 13, and 14. This mainly because of the sensitivity and the stability of the gyroscope is not good enough to perform a perfect sense. So in the future, the structure should be designed more sensitive and the system of the gyroscope should be executed more stable.

7 Conclusions

A tri-axis MEMS gyroscope is proposed in this paper. The operating principle, structure design and performance simulation, fabrication process and circuitry are discussed in detail. Then the implementation of this gyroscope is

executed. The performance is then evaluated by experiment. And the scale factor is about -0.0078 V/°/s, -0.0043 V/°/s and -0.0049 V/°/s, and the nonlinearities are 5.37, 4.91 and 8.66 % along x-, y- and z-axis respectively.

Besides coupling between drive and sense modes, the character of coupling among sense modes of gyroscope are considerable. It means that when the gyroscope rotates along certain sense axis, the scale factor along other sense axis will be affected for the drive movement being affected both in frequency and vibration amplitude. The character of coupling among drive and sense modes is proved both in simulation and experiment. And the results both in simulation and experiment dedicate that the scale factor along certain sense axis decreases when gyroscope rotates on other perpendicular axis.

References

- Chou CS, Chang CO (1997) Modal precession of a hemispherical shell gyro excited by electrostatic field. *Jpn J Appl Phys* 36:7073–7081
- Chou CS, Chang CO, Hwang JJ (1999) Vibration of a hemispherical shell gyro excited by an electrostatic field. *Int J Appl Electromagn Mech* 10:25–449
- Dao DV, Dau VT, Dinh TX, Sugiyama S (2007) A fully integrated MEMS-based convective 3-DOF gyroscope. In: *The 14th international conference on solid-state sensors, actuators and microsystems*, Lyon, France, June 10–14, 2007, pp 1211–1214
- Johari H, Shah J, Ayazi F (2008) High frequency XYZ-axis single-disk silicon gyroscope. In: *MEMS 2008*, Tucson, AZ, USA, January 13–17, 2008, pp 856–859
- John JD, Vinay T (2006) Novel concept of a single-mass adaptively controlled tri-axial angular rate sensor. *IEEE Sensor J* 6:588–595
- Okada K, Matsu Y, Taniguchi N, Itano H (2003) Development of 3-axis gyro-sensor using piezoelectric element. In: *Proceedings of the 20th Sensor Symposium*, pp 123–126
- Tsai N-C, Sue C-Y (2008a) Fabrication and analysis of a micro-machined tri-axis gyroscope. *J Micromech Microeng* 18:115014
- Tsai N-C, Sue C-Y (2008b) Design and analysis of a tri-axis gyroscope micro-machined by surface fabrication. *IEEE Sensors J* 8:1933–1940
- Tsai N-C, Sue C-Y (2010) Experimental analysis and characterization of electrostatic-drive tri-axis micro-gyroscope. *Sens Actuators, A* 158:231–239
- Tsai N-C, Sue C-Y, Lin C-C (2009) Performance characterization of a decoupled tri-axis micro angular rate sensor. *Microsyst Technol* 15:235–249
- Zhang T, Wang W (2012) Design modeling and simulation of a triple-axis MEMS gyroscope. *Inertial sensors and systems*, Karlsruhe, Germany, pp 11.1–11.11
- Zhu R, Ding H, Su Y, Zhou Z (2006) Micromachined gas inertial sensor based on convection heat transfer. *Sens Actuators A* 130(31):68–74